Ionization of N_2, O_2, and linear carbon clusters in a strong laser pulse

A. Jaroń-Becker,[1,2,*] A. Becker,[3,†] and F. H. M. Faisal[2]
[1] *Institute for Theoretical Physics, Warsaw University, Hoza 69, 00-691 Warsaw, Poland*
[2] *Fakultät für Physik, Universität Bielefeld, Postfach 100131, D-33501 Bielefeld, Germany*
[3] *Max-Planck-Institut für Physik komplexer Systeme, Nöthnitzer Strasse 38, D-01187 Dresden, Germany*
(Received 2 September 2003; published 27 February 2004)

Multiphoton ionization of linear molecules is studied using the strong-field *S*-matrix approach. Numerical calculations for the angular distribution and the energy spectrum of the photoelectron as well as the total ionization rates and yields in an intense linearly polarized laser pulse are performed. Results are obtained for molecules aligned along the polarization axis and for ensembles of molecules having a random orientation of the molecular axis with respect to the polarization direction. Signatures of the molecular geometry and the orbital symmetry are identified and discussed with reference to molecular imaging and alignment. It is found that these signatures are clearly marked for the diatomic molecules C_2, N_2, and O_2, but are much weaker for the group of linear carbon clusters due to the polyatomic character as well as to the competing contributions from different valence shells of these molecules. Finally, predictions of the present theory for the dependence of the total ionization rates and yields on the orientation of the molecule are compared with other theoretical models and recent experimental data.

DOI: 10.1103/PhysRevA.69.023410 PACS number(s): 33.80.Rv, 33.80.Wz

I. INTRODUCTION

Currently, there is great interest in exploring the response of molecules to ultrashort intense laser pulses. A variety of multiphoton processes have been observed, including multiphoton ionization, dissociative ionization, multiple ionization, fragmentation, Coulomb explosion, and high harmonic generation. All these processes are characterized by the highly nonlinear interaction between the electrons of the molecule and the external laser field at high intensities (for recent reviews, see e.g., Refs. [1,2]). Single electron ionization is perhaps the most fundamental process among them and occurs often as a precursor of the others.

While the dynamical aspects of ionization of atoms in a strong laser field are considered to be well understood nowadays, theoretical analysis of the same process in more complex targets, such as diatomic and polyatomic molecules, is a topic of active research. Much progress has been made in the development of *ab initio* time-dependent theoretical simulations by direct solution of the Schrödinger equation of the system of interest. Since such calculations require a large space-time grid and, hence, an enormous computational power, current investigations are limited to one- and two-electron molecules, e.g., H_2^+ and H_2 (for recent papers, see e.g., Refs. [3,4]). One way to avoid this obstacle, in order to study more complex diatomic or even polyatomic molecules, is to extend to the molecular case approximation methods, which have been successfully used for the atoms before. Recently, an intense-field many-body *S*-matrix ansatz [5–8] and tunneling ionization models [9–11] have been developed for this purpose.

In this paper we use the first-order term of the *ab initio* *S*-matrix series to investigate the single electron ionization of the diatomics C_2, N_2, O_2, and the linear carbon clusters up to C_9 in an intense laser pulse. This theoretical ansatz has been used before to analyze the influence of interferences of the electronic wave packets from different atomic centers within a diatomic or polyatomic molecule on the total ion yields [5,6] and the electron energy spectrum [7]. For example, it has been shown that the antibonding symmetry [12] of the highest occupied molecular orbital (HOMO) in O_2 gives rise to a destructive interference between the two subwaves, which leads to a suppression of the low-energy part of the above threshold ionization (ATI) spectrum and, consequently, of the total ion yields. Further signatures of molecular symmetry have been identified recently in the yields of doubly ionized polyatomic molecules and its fragments [13], in high harmonic spectra of diatomics [14–16] and ring-shaped molecules [17–19], in high-order ATI spectra of diatomics [20], as well as in photoelectron angular distributions [8].

The purpose of the present paper is to provide a more complete study of the signatures of molecular orbital symmetry and molecular orientation in the photoelectron energy spectra and angular distributions as well as the total ionization rates and yields for laser-induced ionization of linear molecules. The paper is organized as follows: First, we briefly sketch the *S*-matrix ansatz, used for the present analysis, as well as the geometrical structure of the molecules investigated and the symmetries of the different classes of orbitals in a linear molecule. Next, signatures of molecular orbital symmetry are identified in the angular distributions and the energy spectra of the photoelectron considering the diatomics C_2, N_2, and O_2 as examples. Supplementary analysis for the group of small linear carbon clusters demonstrates the role of competing contributions from different valence orbitals in more complex polyatomic molecules. A comparison of the results obtained for ensembles of mol-

*Present address: Max-Planck-Institut für Physik komplexer Systeme, Nöthnitzer Str. 38, D-01187 Dresden, Germany. Electronic address: jaron@mpipks-dresden.mpg.de
†Electronic address: abecker@mpipks-dresden.mpg.de

ecules, which are aligned with their internuclear axis along the polarization direction, with those for sets of randomly oriented molecules provides information for identification of molecular alignment. Finally, we apply the theory to analyze the dependence of total ionization rates and yields on the orientation of the molecular axis, and compare the results with those of other theoretical approaches and recent experimental data.

II. THEORY

A. Rates and yields

For our analysis we have used an extension of the so-called Keldysh-Faisal-Reiss model [21–23], which is obtained as the leading-order term of an *S*-matrix expansion. It involves a transition matrix element between the initial-state wave function of a bound state of the molecule, $|\Phi_i\rangle$, and the product state of the Volkov wave function of the emitted electron in the field and the unperturbed final bound-state wave function of the residual molecular ion, $|\Phi_f^+\rangle$, and is corrected approximately for the long-ranged Coulomb interaction in the final state [24]. The *doubly differential rate* of ionization *per* molecule, and per element of solid angle $d\Omega$, from an active orbital with N_e equivalent electrons, on absorbing N photons from a linearly polarized laser field is given by [5,6]

$$\frac{dW_{fi}^{(N)}(I,\hat{n})}{d\Omega} = 2\pi N_e C_{coul} k_N (U_p - N\omega)^2 \times J_N^2\left(\boldsymbol{\alpha}_0\cdot\boldsymbol{k}_N, \frac{U_p}{2\omega}\right)|\langle\phi_{\boldsymbol{k}_N}\Phi_f^+|\Phi_i\rangle(\hat{n})|^2. \tag{1}$$

$C_{coul}=[(2I_p)^{3/2}/E_0]^{2Z/\sqrt{2I_p}}$ is a Coulomb factor accounting for the interaction of the emitted electron with the residual ion of charge state $Z=1$ [25]. E_0 is the peak field strength of the laser and I_p is the ionization energy of the molecule. $J_N(a;b)$ is a generalized Bessel function of two arguments (e.g., Refs. [23,26]), where $\alpha_0=\sqrt{I}/\omega$ is the quiver radius and $U_p=I/4\omega^2$ is the quiver energy of an electron in a laser field of frequency ω and intensity I. $k_N^2/2=N\omega-U_p-I_p$ is the kinetic energy of an electron on absorption of N photons from the field.

Orientation of the molecular axis in space is determined in Eq. (1) via the unit vector $\hat{n}$. Hence, any distribution of molecular axis in an ensemble of molecules is taken into account by averaging the rates over the angles $(\theta_{\hat{n}},\phi_{\hat{n}})$.

By summation over the number of photons absorbed from the field one readily gets from Eq. (1) the *differential ionization rate* per element of solid angle $d\Omega$,

$$\frac{dW_{fi}(I,\hat{n})}{d\Omega} = \sum_{N=N_0}^{\infty} \frac{dW_{fi}^{(N)}(I,\hat{n})}{d\Omega}, \tag{2}$$

where N_0 is the minimum (or threshold) photon number. Integration of Eq. (1) over the ejection angles only gives the photoelectron angular distribution for a given ATI channel,

$$W_{fi}^{(N)}(I,\hat{n}) = \int d\Omega \frac{dW_{fi}^{(N)}(I,\hat{n})}{d\Omega}. \tag{3}$$

The *total ionization rate* per molecule is obtained by adding the contribution from all channels,

$$\Gamma_{fi}(I,\hat{n}) = \sum_{N=N_0}^{\infty} \int d\Omega \frac{dW_{fi}^{(N)}(I,\hat{n})}{d\Omega}. \tag{4}$$

Generally speaking, experimental data for the rate of ionization *per* molecule are not available, and hence a comparison of theory and experiment is not practicable as yet at this basic level. Experimental data are usually obtained (in a relative scale) in terms of the distributions of ionization *yields* in the interaction volume for the ensemble of molecules in the laser focus. It is therefore necessary to construct the respective distributions of ionization yields theoretically to facilitate the comparison. Angular and energy distributions for photoelectron as well as ion yields are determined by combining the fundamental rates, Eqs. (1)–(4), with the rate equations governing the respective populations at any point in the laser focus, and adding the contributions from all points.

Let the normalized population of the neutral molecules at a point $(\mathbf{r},t)$, having the orientation $\hat{n}$, be $P_0(\mathbf{r},t,\hat{n})$, and that of the ions be $P(\mathbf{r},t,\hat{n})$. The populations of the neutral and the ionized species are then governed by the rate equations,

$$\frac{dP_0(\mathbf{r},t,\hat{n})}{dt} = -\Gamma_{fi}(I(\mathbf{r},t),\hat{n})P_0(\mathbf{r},t,\hat{n}), \tag{5}$$

$$\frac{dP(\mathbf{r},t,\hat{n})}{dt} = \Gamma_{fi}(I(\mathbf{r},t),\hat{n})P_0(\mathbf{r},t,\hat{n}). \tag{6}$$

The respective partial yields (angular and energy distributions) are governed by

$$\frac{dP_\Omega(\boldsymbol{r},t,\hat{n})}{dt} = \frac{dW_{fi}(I(\mathbf{r},t),\hat{n})}{d\Omega}P_0(\mathbf{r},t,\hat{n}), \tag{7}$$

$$\frac{dP^{(S)}(\boldsymbol{r},t,\hat{n})}{dt} = W_{fi}^{(S)}(I(\mathbf{r},t),\hat{n})P_0(\mathbf{r},t,\hat{n}), \tag{8}$$

where $P_\Omega(\boldsymbol{r},t,\hat{n})\equiv dP(\boldsymbol{r},t,\hat{n};\Omega)/d\Omega$ stands for the angular distribution; $P^{(S)}(\boldsymbol{r},t,\hat{n})$ is the (discrete) energy distribution corresponding to the ATI channels $(S=N-N_0=0,1,2,\ldots)$. Note that the last two equations determining the respective partial distributions are consistent with the equation of the total ionization, as can be readily seen by considering the integration over the solid angle $d\Omega$, or the summation over the ATI-index S, and comparing the result with the equation satisfied by the total ion yield,

$$P(\mathbf{r},t,\hat{n}) = \int d\Omega \frac{dP(\boldsymbol{r},t,\hat{n};\Omega)}{d\Omega} \tag{9}$$

$$= \sum_{S=0}^{\infty} P^{(S)}(\mathbf{r},t,\hat{n}). \quad (10)$$

The above system of rate equations is solved with the initial conditions $P_0(\mathbf{r},t=-\infty,\hat{n})=1$ and $P(\mathbf{r},t=-\infty,\hat{n})=0$, as well as $P_\Omega(\mathbf{r},t=-\infty,\hat{n})=0$ (for all Ω) and $P^{(S)}(\mathbf{r},t=-\infty,\hat{n})=0$ (for all S). We note that the assumed normalization of population, $P_0(\mathbf{r},t,\hat{n})+P(\mathbf{r},t,\hat{n})=1$, is satisfied at all space-time points $(\mathbf{r},t)$ in the laser focus, as can be easily seen by adding the first two rate equations and using the respective initial conditions. For the actual computations we have used, as usual, a Gaussian pulse profile (pulse duration, τ) centered around $t=0$, and a TEM_{00}-mode Gaussian beam.

We may observe that the rate concept and the use of rate equations become useful, when the ionization process is adiabatic. In the case of ionization of atoms the onset of adiabaticity has been found to occur for pulse durations as short as about three cycles of the field [25]. We assume that this adiabatic rate condition holds for molecules as well. Therefore, all pulse lengths used in the present calculations are chosen to exceed the threshold of three cycles. The signatures of the molecular orbital symmetry and molecular orientation, presented below, are found to be rather insensitive to variations of the pulse lengths up to 100 fs.

This theory has been used previously to analyze the phenomenon of suppressed molecular ionization in diatomics [5,7] and in symmetric hydrocarbons [6]. The predictions of the theory for the ion yields and the above-threshold ionization spectra have been found to be in good agreement with the experimental data for N_2, O_2, C_2H_2, C_2H_4, and C_6H_6, but not for the highly electronegative molecule F_2 [27,28]. We have therefore restricted our analysis to linear molecules of C, N, and O atoms. Particularly, the successful application to the hydrocarbons lets one to expect that the theory provides reliable predictions for carbon clusters as well.

B. Orbitals and geometrical structure

Ionization potentials and internuclear distances for the diatomics C_2, N_2, and O_2 have been taken from Ref. [29]. The structures and equilibrium geometries of the carbon clusters were the subject of a lively discussion in literature since the development of *ab initio* chemical programs. Only recently, mostly due to increasing computer power, an agreement on the equilibrium geometry was obtained [30,31]. We have made use of recent results for the vertical ionization potentials [32] and the structure of the carbon chains [30,32]. Tables I and II display the ionization energies of the HOMO and inner valence shells and the bond lengths of the diatomics and linear carbon clusters, used in the present calculations. We have obtained wave functions for the neutral molecule in the initial state and the molecular ion in the final state using the GAMESS-US program [33] and the geometric structures in Table II as input data, within the Hartree-Fock approximation.

The sample of diatomics used in the present analysis allows us to analyze systematically the influence of the orbital symmetry on the photoelectron and ion yields, since the HOMOs of C_2, N_2, and O_2 belong to three classes of orbital symmetries, namely, π_u, σ_g, and π_g. Thus, basic signatures of π vs σ, gerade vs ungerade, as well as bonding vs antibonding symmetry of an orbital can be studied qualitatively within this group of diatomics.

TABLE I. Ionization potentials I_p in eV for the outermost and inner valence shell orbitals of the diatomics [29] as well as of the linear carbon clusters [32].

C_2	$1\pi_u$	$2\sigma_u$		
	11.41	15.40		
N_2	$2\sigma_g$			
	15.58			
O_2	$2\pi_g$	$2\pi_u$	$2\sigma_g$	
	12.07	16.10	18.17	
C_3	$3\sigma_u$	$4\sigma_g$	$1\pi_u$	
	11.920	12.739	12.879	
C_5	$1\pi_g$	$5\sigma_u$	$6\sigma_g$	$1\pi_u$
	11.006	11.404	11.486	12.651
C_7	$2\pi_u$	$7\sigma_u$	$8\sigma_g$	$1\pi_g$
	9.906	10.821	10.829	11.579
C_9	$2\pi_g$	$10\sigma_g$	$9\sigma_u$	$2\pi_u$
	9.167	10.397	10.397	12.141

Carbon clusters, on the other hand, belong to a group of molecules with a large variety of structural forms. Due to the bonding flexibility of carbon, its ability to form stable single, double, or triple bonds, carbon clusters appear as chains, monocyclic or polycyclic rings, cages, bowls, graphitic sheets, or graphite nanotubes. Already the subgroup of carbon clusters with less than 10 carbon atoms is divided into two sets, namely, molecules with the even number of carbon atoms have the shape of the ring while molecules with odd number of carbon atoms appear as chainlike structures [30,31]. Thus, the group of small linear clusters opens the opportunity to analyze whether or not the basic signatures of orbital symmetry identified for the diatomics appear for linear polyatomics with a more complex structure as well.

We may also note that carbon clusters are important for many diverse branches of science, e.g., astrophysics, chemistry of carbon stars, combustion processes, and material sciences [30,31]. In this context the optical response of carbon clusters has been recently studied as a diagnostic tool for the

TABLE II. Equilibrium internuclear distances in angstroms for the diatomics [29] and the linear carbon clusters, starting from the outermost C atom towards the middle [30].

C_2	1.2425			
N_2	1.09768			
O_2	1.20152			
C_3	1.2943			
C_5	1.2896	1.2819		
C_7	1.290	1.286	1.272	
C_9	1.29	1.294	1.275	1.281

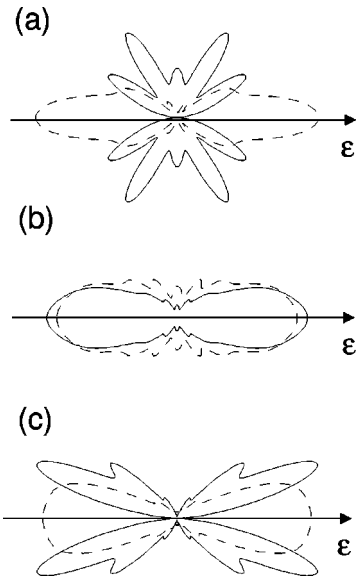

FIG. 1. Angular distributions for the diatomic molecules (a) C_2 ($I_0=5\times10^{13}$ W/cm^2), (b) N_2 ($I_0=10^{14}$ W/cm^2), and (c) O_2 ($I_0=10^{14}$ W/cm^2). A comparison is shown between the results obtained for aligned orientation (solid lines) and those for random orientation (dashed lines). Please note that the results are not shown on the same scale. Other laser parameters: $\lambda=800$ nm, $\tau=10$ fs.

structure of carbon clusters [34,35]. Thus, an analysis of the interaction of carbon clusters with a strong external field may also contribute to the knowledge of their physical and chemical properties as well as to the understanding of a large variety of chemical processes.

III. DIFFERENTIAL SPECTRA

In this section we apply the present model to investigate the angular distributions and the energy spectra of the photoelectron. Results obtained for the two limiting cases of molecular alignment will be compared, namely, random orientation of the molecular axis and its complete alignment along the polarization direction.

A. Angular distributions

Calculations for the photoelectron angular distributions have been performed using Eqs. (2), (5), and (7). In Fig. 1 we present the results for the diatomic molecules (a) C_2, (b) N_2, and (c) O_2 for a wavelength of $\lambda=800$ nm and a pulse duration of $\tau=10$ fs; the laser peak intensity was $I_0=5\times10^{13}$ W/cm^2 (for C_2) and $I_0=10^{14}$ W/cm^2 (for N_2 and O_2) respectively. In the figures, the polar angles are measured from the laser polarization $\boldsymbol{\varepsilon}$ in the laboratory frame. Distributions obtained for random orientation of the molecular axis (dashed lines) are compared with those for molecules aligned with their axis parallel to the polarization direction (solid lines).

It is seen from the figure that the angular distributions show a minimum along the polarization direction, if molecules having the HOMO of π symmetry are assumed to be completely aligned along the polarization axis [cf. Figs. 1(a) C_2 and 1(c) O_2, solid lines]. This is a consequence of the symmetry of the molecular ground state and can be understood as follows [8]. Molecular orbitals of π symmetry, like the HOMOs of C_2 and O_2, possess a nodal plane through the (body-fixed) molecular axis leading to a vanishing photoelectron angular distribution along this axis. In a randomly oriented ensemble of such linear molecules (cf. dashed lines) this minimum is washed out by the addition of the contributions from the overwhelmingly larger number of molecules that are not oriented along the space-fixed axis. In contrast, in the case of N_2 molecules the HOMO is of σ symmetry, which does not have a nodal plane along the molecular axis, and hence the distribution is qualitatively the same in both cases of orientation [cf. Fig. 1(b)]. Please note, that for the diatomics contributions from the inner orbitals are found to be negligible for all the results (angular distributions, energy spectra, total ionization rates, as well as ion yields) presented in this paper.

The characteristic dependence of the angular distributions on the molecular orientation for diatomic molecules having active orbitals of π symmetry may in turn provide a simple means to determine the presence of spatial alignment in an ensemble of molecules. Please note that it has been shown previously [8] that the minimum appears as the alignment is decreased below a cone angle of about 30°. We may also note that our results confirm earlier findings at moderate laser intensities that photoelectron angular distributions provide a sensitive test of the molecular structure and symmetry (for recent reviews, see, e.g., Refs. [36,37]). This concept is also used to investigate excited-state dynamics via femtosecond time-resolved photoelectron spectroscopy in excitation-ionization experiments [38].

The above interpretation is applicable to photoelectron emission from any orbital of π symmetry in a linear molecule. However, signatures such as the characteristic minimum along the polarization axis may not show up for every polyatomic molecule. This is due to the more complex electronic structure of polyatomics, in which contributions from several valence orbitals, which are energetically very close, can contribute to the total angular distribution. In order to illustrate this, we present in Fig. 2 angular distributions for the set of linear odd-numbered carbon clusters: (a) C_3, (b) C_5, (c) C_7, and (d) C_9. A comparison is shown between the results of the full calculations, in which all valence shells are taken into account (panels on the left-hand side), and those for which the electron emission from the HOMO is considered only (panels on the right-hand side). As expected a node along the polarization direction appears as a characteristic signature of complete alignment in the distributions arising from the HOMO of those three carbon clusters having an outermost orbital of π symmetry [cf. Figs. 2(b) C_5, 2(c) C_7, and 2(d) C_9]. But, at the given laser parameters we observe for C_5 and C_9 that the minimum turns into a maximum, when the contributions from the other valence shells are added [cf. left-hand panels of Figs. 2(b) and 2(d)], due to the dominant contributions from the inner valence shells of σ symmetry in these cases. Thus, the signature of alignment manifested as a minimum along the polarization direction for the diatomics

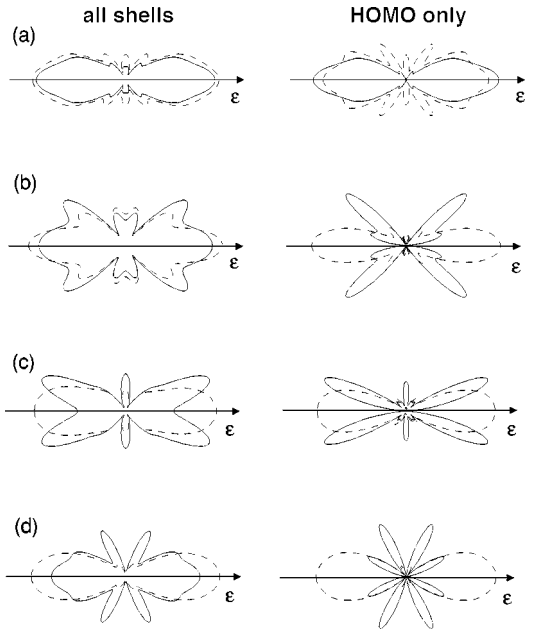

FIG. 2. Angular distributions for linear carbon clusters: namely, (a) C_3, $I_0=5\times10^{13}$ W/cm^2; (b) C_5, $I_0=2\times10^{13}$ W/cm^2; (c) C_7, $I_0=2\times10^{13}$ W/cm^2; and (d) C_9, $I_0=10^{13}$ W/cm^2. Panels on the left-hand side show the results, when contributions from all valence shells are taken into account, while those on the right-hand side show the distributions arising from the HOMO only. Please note that the results are not shown on the same scale. The rest as in Fig. 1.

is not unconditionally applicable in the case of linear polyatomic molecules.

During the course of the calculations it has been found that the angular distributions qualitatively do not change with the change of the laser wavelength. In order to illustrate this behavior we present in Fig. 3 results for O_2 and C_7 at 1600 nm and 2400 nm. In particular, we note that for the diatomic O_2 the node along the polarization direction as a signature of alignment is present at all wavelengths investigated. We may further note that the angular distributions become narrower around the polarization direction with the increase of the wavelength due to the increase of the degree of nonlinearity of the ionization process with increasing wavelength.

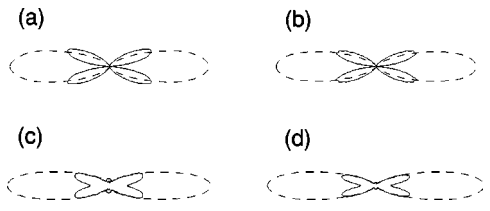

FIG. 3. Angular distributions for O_2 and C_7 at two longer wavelengths, namely (a) O_2, $\lambda=1600$ nm; (b) O_2, $\lambda=2400$ nm, $I_0=10^{14}$ W/cm^2; (c) $C_7=1600$ nm; and (d) C_7, $\lambda=2400$ nm, $I_0=2\times10^{13}$ W/cm^2. Other laser parameter: $\tau=50$ fs.

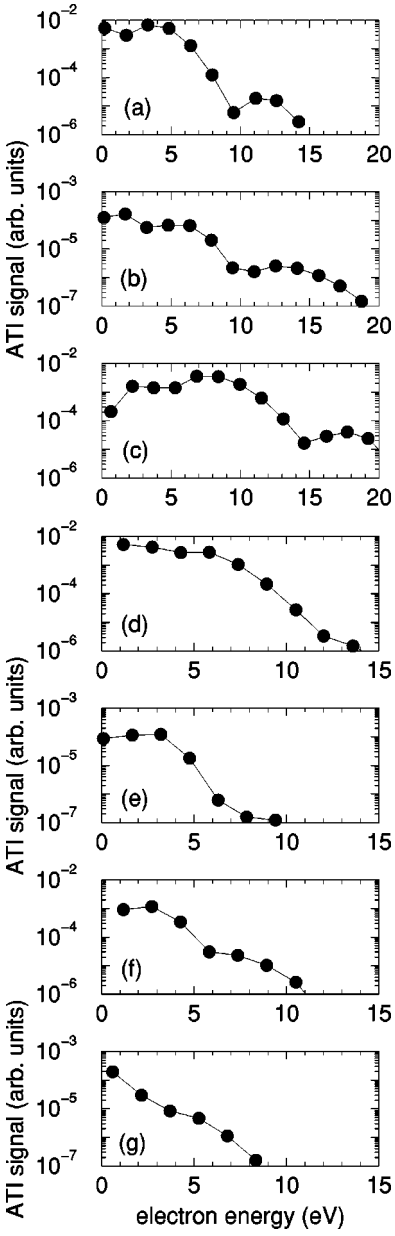

FIG. 4. Energy spectra for emission of the electron along the polarization direction and random orientation of the molecular axis: (a) C_2, $I_0=5\times10^{13}$ W/cm^2; (b) N_2, $I_0=10^{14}$ W/cm^2; (c) O_2, $I_0=10^{14}$ W/cm^2; (d) C_3, $I_0=5\times10^{13}$ W/cm^2; (e) C_5, $I_0=2\times10^{13}$ W/cm^2; (f) C_7, $I_0=2\times10^{13}$ W/cm^2; and (g) C_9, $I_0=10^{13}$ W/cm^2. Other laser parameters: $\lambda=800$ nm, $\tau=10$ fs.

B. Electron energy spectra

The present theoretical model has been applied previously [7] to analyze the qualitative signatures of the interference effects induced by the ''bonding'' vs ''antibonding'' symmetry [12] of the molecular ground state on the photoelectron energy spectrum or ATI spectrum of diatomic molecules. We may recall that the lowest ATI peaks of a homonuclear diatomic having an active orbital of antibonding symmetry, such as O_2 (π_g symmetry), have been found to be suppressed by a destructive interference effect. This can be

readily understood from Eq. (3), when written more explicitly as

$$W_{fi}^{(N)}(I,\hat{n}) = 2\pi N_e C_{coul} \sum_{N=N_0}^{\infty} \int d\hat{\mathbf{k}}_N k_N (U_p - N\omega)^2 \times J_N^2\left(\boldsymbol{\alpha}_0 \cdot \mathbf{k}_N, \frac{U_p}{2\omega}\right) F(\mathbf{k}_N) \times \begin{cases} \sin^2(\mathbf{k}_N \cdot \mathbf{R}/2) & \text{for antibonding symmetry,} \\ \cos^2(\mathbf{k}_N \cdot \mathbf{R}/2) & \text{for bonding symmetry,} \end{cases} \tag{11}$$

if the diatomic molecular orbital is expressed in the convenient linear combination of atomic orbitals representation:

$$\Phi_i(\boldsymbol{r};\boldsymbol{R}_1,\boldsymbol{R}_2) = \sum_{j=1}^{j_{max}} a_j \phi_j(\boldsymbol{r},-\boldsymbol{R}/2) + b_j \phi_j(\boldsymbol{r},\boldsymbol{R}/2), \tag{12}$$

where ϕ_j are the atomic orbitals and R is the internuclear distance. $F(\mathbf{k}_N)$ is a function of $\mathbf{k}_N$ and of the atomic orbitals, and is independent of the molecular symmetry. The interference effects due to the antibonding vs bonding symmetry [12] occur in Eq. (11) via the trigonometric factors $\sin^2$ and $\cos^2$.

Figure 4 shows the calculated ATI spectra for the diatomics (a)–(c) and the carbon clusters (d)–(g) for the ejection of the photoelectron along the polarization axis and randomly oriented ensembles of molecules. Laser parameters are $\lambda = 800$ nm and $\tau = 10$ fs, while the peak intensity differs from molecule to molecule (see figure caption). The suppression of the lowest-order ATI peaks is clearly present in the spectrum of O_2 (panel *c*, antibonding π_g symmetry) as compared to those of C_2 (panel *a*, bonding π_u symmetry) and N_2 (panel *b*, bonding σ_g symmetry) where no suppression is seen in accordance with the present theory.

The energy spectra of the carbon clusters on the other hand do not show any characteristic signature of orbital symmetry [cf. Figs. 4(d)–4(g)]. This is due to two reasons: First, the bonding vs antibonding symmetry [12] does not apply for the set of carbon clusters, since that symmetry in the present case is broken by the presence of an unpaired carbon atom in the middle of the chain. In particular, if the electron probability density in the orbital is strongly localized around the center atom interference between the pairs of other atoms is disturbed. Second, the contributions from valence shells of different symmetry add up to the full energy spectra in the case of the carbon clusters. Consequently, any signature of suppression near the threshold of the ATI spectra, even for those clusters having a HOMO of antibonding symmetry such as C_5 and C_9, gets lost.

Equation (11) suggests further that energy spectra of homonuclear diatomic molecules may be suppressed not only near the threshold but also at certain higher-energy values given by

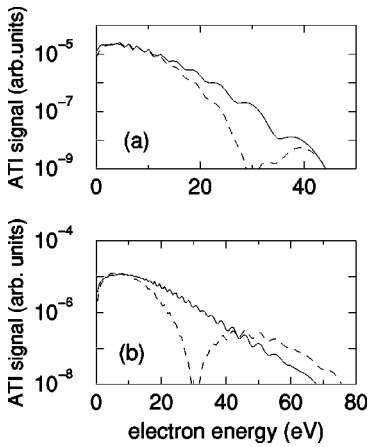

FIG. 5. Energy spectra of N_2 for photoelectron emission along the polarization direction at $I_0 = 10^{14}$ W/cm^2, $\tau = 50$ fs, and (a) $\lambda = 1600$ nm and (b) $\lambda = 2400$ nm. Predictions of the present theory for a set of randomly oriented molecules (solid lines) and for completely aligned molecules (dashed lines) are compared.

$$\frac{k_N^2}{2} = \frac{2}{R^2(\hat{k}_N \cdot \hat{n})^2} \begin{cases} n^2\pi^2 & \text{for antibonding symmetry,} \\ n^2\pi^2/4 & \text{for bonding symmetry,} \end{cases} \tag{13}$$

with $n = 1,2,3,\ldots$. The above values depend on the internuclear distance as well as on the directions of the electron emission, $\hat{k}_N$, and of the orientation of the molecular axis, $\hat{n}$. Thus, the suppression should be most clearly visible for fixed directions of $\hat{k}_N$ and $\hat{n}$.

In order to test this expectation we have performed calculations of the ATI spectra of N_2 (bonding σ_g symmetry) for emission of the photoelectron along the polarization direction. In Fig. 5 we present a comparison of the results for aligned (dashed lines) and random orientation (solid lines) of the molecule at two different laser wavelengths, (a) 1600 nm and (b) 2400 nm. As expected, in the case of complete alignment a deep minimum appears around 31 eV at both laser wavelengths. In contrast, in the case of random orientation the energy spectra are relatively smooth and, in particular, there is no minimum due to the averaging over the molecular orientations with respect to the fixed direction of photoelectron emission. Thus, the minimum in the ATI spectra at higher electron energies can be considered as another trace of the interference effects but even more of molecular alignment. Detection of this minimum can be further useful in view of molecular imaging, since its position in the energy spectrum determines the internuclear distance.

IV. TOTAL IONIZATION RATES AND ION YIELDS

Most of the experiments on molecular ionization have been performed with randomly oriented molecules. Only very recently, it has become possible to measure total ion yields for ensembles of molecules showing a maximum alignment either along or perpendicular to the polarization direction [39]. The experimental data support theoretical predictions [9–11,40,41] that the total ionization rates of neutral

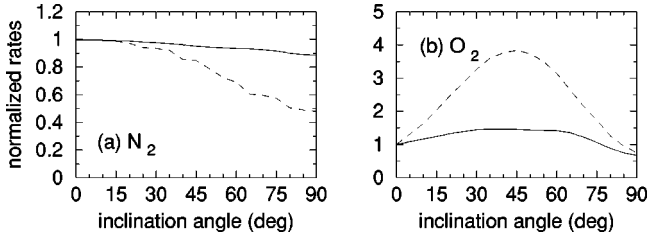

FIG. 6. Total ionization rates of (a) N_2 and (b) O_2 as a function of the inclination angle between the molecular axis and the polarization axis of a linearly polarized laser field at $\lambda = 800$ nm and two intensities, 2×10^{13} W/cm^2 (solid lines) and 3.2×10^{14} W/cm^2 (dashed lines). The results are normalized with respect to the rates at 0°.

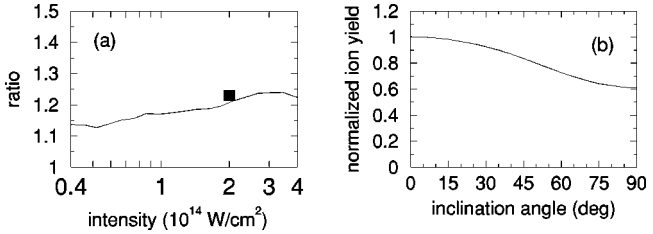

FIG. 7. (a) Ratio of total ion yields for two ensembles of prealigned N_2 molecules as a function of the peak intensity (see text) and (b) total ion yields as a function of the inclination angle between the molecular axis and the polarization axis of a linearly polarized laser pulse. Laser parameters: $\lambda = 800$ nm, $\tau = 45$ fs, $I_0 = 2\times10^{14}$ W/cm^2.

diatomic molecules depend on the inclination angle between the molecular axis and the field polarization.

In Fig. 6 we present total ionization *rates* [c.f. Eq. (4)] of (a) N_2 and (b) O_2 as a function of the angle between the polarization direction and the molecular axis. Results are obtained for $\lambda = 800$ nm and two intensities, namely, 2×10^{13} W/cm^2 (solid lines) and 3.2×10^{14} W/cm^2 (dashed lines). The comparison shows that for N_2 the ionization rates decrease monotonically with increasing inclination angle, while those for O_2 have a maximum at about 45° and are at minimum for alignment along and perpendicular to the polarization axis.

Qualitatively, the predictions of the present theory on the dependence of the rates on the inclination angle agree with the results from the molecular tunneling theory by Zhao *et al.* [11]. The results can be simply understood in terms of the orientation of the electronic density of the molecular ground states with respect to the field direction [11]. In a strong linearly polarized laser field the rate of ionization is expected to be maximum, if the maximum of the electronic density is aligned along the polarization direction. This is reached for alignment of the molecular axis along the polarization direction in the case of N_2 (σ_g orbital), and for an angle of about 45° between the molecular axis and the polarization direction for O_2 (π_g orbital), which is in agreement with the results in Fig. 6. Photoelectron emission in a linearly polarized laser field is also expected to become more strongly directed along the polarization direction with increasing field intensity. Thus, following the above interpretation, one may expect that any orientation dependence of the total ionization rates becomes stronger as the field intensity increases. The results shown in Fig. 6 are consistent with this expectation, however, the dependence on the laser intensity is in contradiction to those in Ref. [11].

Next, we analyze recent experimental data on alignment-dependent strong-field ionization of N_2 in an intense laser pulse obtained by Litvinyuk *et al.* [39]. Ion yields have been measured for two ensembles of molecules with a maximum alignment along and perpendicular to the field direction. The distributions of the molecular axis in the two ensembles are determined by [39]

$$F_1(\theta_n^{\wedge}) = A\{\cos^2(\theta_n^{\wedge}) + [1.692\sin(\theta_n^{\wedge})]^2\}^{-1/2} - 0.415$$

(maximum alignment along the field direction),

$$F_2(\theta_n^{\wedge}) = B\{\cos^2(\theta_n^{\wedge}) + [0.929\sin(\theta_n^{\wedge})]^2\}^{-1/2} - 0.916$$

(maximum alignment perpendicular to the field direction),

where A and B are normalization coefficients and $\theta_n^{\wedge}$ is the angle between the molecular axis and the polarization direction (the distributions are assumed to be symmetric with respect to the polar angle about the field direction). We have performed calculations of the ion *yields*, using Eqs. (4)–(6) together, for both ensembles. The ratio of the yields obtained for the ensemble, described by the distribution F_1, to those obtained for the second ensemble is shown in Fig. 7(a) as a function of the peak laser intensity. Other laser parameters in the experiment [39] and in the calculations are $\lambda = 800$ nm and $\tau = 40$ fs. The theoretical results show quite generally, in agreement with the experimental data (solid square), that N_2 molecules aligned along the field direction are easier to ionize than those aligned perpendicular to it. This is further confirmed by the results in Fig. 7(b), where the present predictions for the ion yields of N_2 at $I_0 = 2\times10^{14}$ W/cm^2 are plotted as a function of the angle between the molecular axis and the polarization direction. It is seen that at these laser parameters the ionization probability for N_2 is 1.67 times larger when the molecular axis is aligned along the field direction than if it is aligned perpendicular to it.

We have also investigated the orientation dependence of the ion yields of the linear carbon clusters as a function of the peak intensity. It is found that the yields depend rather weakly on the orientation of the molecular axis. To illustrate this point we present in Fig. 8(a) for C_3 (solid line) and C_7 (dashed line) the ratios of the ion yields assuming alignment along the field direction to those for randomly oriented clusters ($\lambda = 800$ nm, $\tau = 100$ fs). For the sake of possible comparison with future experiments we also present here the ion yields of the set of small linear clusters, obtained with the same field parameters, in Fig. 8(b).

Before discussing them further, we may call the reader's attention to a rather subtle aspect of these results, i.e., the change in the slope of the ion yields of C_3 and C_5 at about 2×10^{13} W/cm^2, which are signatures of pronounced *channel closings* [42]. Channel closings are usually difficult to detect in ion yields due to the average over the temporal and

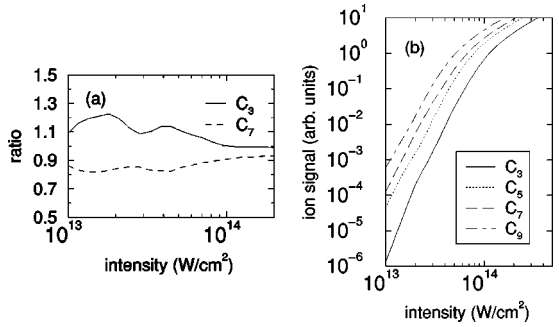

FIG. 8. (a) Ratio of total yields of carbon clusters aligned along the field direction to those of randomly oriented carbon clusters and (b) total yields for carbon clusters aligned along the field direction as functions of the peak intensity. Other laser parameters: $\lambda = 800$ nm, $\tau = 100$ fs.

spatial intensity profiles. For the diatomic molecules and linear carbon clusters we have found, in the course of our analysis, that channel closings are very pronounced for ionization from σ orbitals at low intensities, but not from π orbitals. Moreover out of the two types of σ orbitals the channel closings are found to be stronger for σ_g orbitals than for σ_u orbitals.

The important role of inner valence shells on the total ion yields of the linear clusters is quantified by the results in Fig. 9, where the ratios of the partial yields arising due to ionization from individual orbitals to the total ion yields are plotted as a function of the peak intensity. Please note that the contribution from the HOMO is shown by a solid line in each case, while the styles of other lines distinguish the symmetry of the other contributing orbitals (see figure legend). In general it is seen that for each cluster contributions from at least three orbitals are effective. This illustrates why signatures in the angular distributions and energy spectra due to the symmetry of an individual HOMO orbital (bonding vs antibonding or σ vs π) are found to be washed out for the carbon clusters. Modulations in the contributions from different valence shells (cf. Fig. 9) are due to the channel closings mentioned above. It is worthwhile to recall that unlike in these cases, the contributions from the inner shells for the three diatomics investigated above are found to be smaller than 1% and hence negligible. We may finally also note that for C_5, where the three outermost orbitals are energetically very close together (cf. Table I), ionization from the two inner σ orbitals is in fact stronger than the contribution from the HOMO of π symmetry.

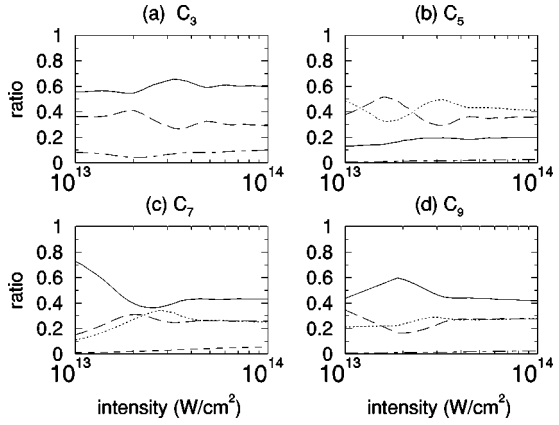

FIG. 9. Contributions of partial yields due to the ionization from individual orbitals to the total ion yields of carbon clusters, (a) C_3, (b) C_5, (c) C_7, (d) C_9, are shown as a function of the peak intensity. The contribution from the HOMO is always shown by a solid line, while the contributions from the inner shells are respectively presented by π_g orbital (dashed line), σ_u orbital (dotted line), π_u orbital (dot-dashed line), and σ_g orbital (long-dashed line). Laser parameters: $\lambda = 800$ nm, $\tau = 100$ fs.

V. CONCLUSIONS

In this paper we have used the intense-field *S*-matrix method to study the ionization of the diatomics C_2, N_2, and O_2 as well as of small linear carbon clusters up to C_9 in a linearly polarized laser pulse. Predictions for the angular distributions and the energy spectra of the photoelectron as well as for the total ionization rates and yields are made. In each case the dependence of the distributions on the orientation of the molecule as well as the influence of ionization from inner valence shells are investigated.

Several symmetry-induced signatures are identified in the partial distributions for the diatomics. First, the angular distribution for diatomics having a HOMO of π symmetry exhibits a node for the emission of the photoelectron along the polarization direction, when the molecule is aligned along the field direction, but not if the molecular axis is randomly oriented. Second, suppression of the energy spectra at the threshold for ionization from a HOMO of antibonding symmetry and at specific higher energies appears due to destructive interference effects between the subwaves of the electron from the two atomic centers in the diatomic. While the suppression near the threshold appears for all orientations of the molecular axis, those at higher energies depend on the inclination angle of the molecular axis, i.e., the angle between the alignment of the molecular axis and the field polarization direction. It is discussed how both the characteristics, i.e., the node in the angular distribution and the suppression of the energy spectra at higher electron energies, can serve as signatures to identify alignment of an ensemble of molecules. Furthermore, it is pointed out that the pronounced minima in the energy spectra may be used for imaging of molecular structure, in particular, at the internuclear distance attained by the molecule at the moment of ionization. The dependence of the distributions on the pulse duration is found to be rather weak for pulse lengths between three cycles of the field and about 100 fs.

Analysis of the results for the linear carbon clusters reveals that the symmetry dependent signatures observed for the diatomics are not unconditionally applicable for larger polyatomic molecules. This is, in particular, due to the competition of contributions from the HOMO and the lower molecular orbitals down to three valence shells of different symmetries in the carbon clusters. Consequently, any signature of a specific symmetry effect of the HOMO is washed out. In contrast, for the diatomics investigated in this paper, the influence of ionization from inner shells is found to be negli-

gible which permits the symmetry of the HOMO to retain its signatures in the observables of the ionization process.

To test the present theory for the dependence of the total ionization rates and yields on the orientation of the molecule we have compared its predictions with the observation in a recent experiment. A good agreement is found which confirms that N_2 molecules which are aligned along the field direction are easier to ionize than those aligned perpendicular to it. In contrast, for O_2 the ionization rates become maximum at an inclination angle of about 45° between the molecular axis and the field direction. Orientation dependence of the rates is predicted to become stronger with increasing field intensity, which is consistent with the highly nonlinear nature of the process, but is in contradiction to an earlier theoretical result.

Pronounced changes of the slope of the ion yields of the linear carbon clusters, due to channel closings, are predicted for ionization from σ orbitals, but not from π orbitals. Finally, ion yields as a function of field intensity are also presented for possible future experimental reference.

ACKNOWLEDGMENT

A.J.-B. acknowledges support via the Alexander von Humboldt-Stiftung (Bonn, Germany).

[1] *Molecules in Laser Fields*, edited by A.D. Bandrauk (Marcel Dekker, New York, 1994).
[2] *Molecules and Clusters in Intense Laser Fields*, edited by J. Posthumus (Cambridge University Press, Cambridge, 2001).
[3] A.D. Bandrauk, S. Chelkowski, and I. Kawata, Phys. Rev. A **67**, 013407 (2003).
[4] K. Harumiya, H. Kono, Y. Fujimura, I. Kawata, and A.D. Bandrauk, Phys. Rev. A **66**, 043403 (2002).
[5] J. Muth-Böhm, A. Becker, and F.H.M. Faisal, Phys. Rev. Lett. **85**, 2280 (2000).
[6] J. Muth-Böhm, A. Becker, S.L. Chin, and F.H.M. Faisal, Chem. Phys. Lett. **337**, 313 (2001).
[7] F. Grasbon, G.G. Paulus, S.L. Chin, H. Walther, J. Muth-Böhm, A. Becker, and F.H.M. Faisal, Phys. Rev. A **63**, 041402(R) (2001).
[8] A. Jaroń-Becker, A. Becker, and F.H.M. Faisal, J. Phys. B **36**, L375 (2003).
[9] M.J. DeWitt, B.S. Prall, and R.J. Levis, J. Chem. Phys. **113**, 1553 (2000).
[10] X.M. Tong, Z.X. Zhao, and C.D. Lin, Phys. Rev. A **66**, 033402 (2002).
[11] Z.X. Zhao, X.M. Tong, and C.D. Lin, Phys. Rev. A **67**, 043404 (2003).
[12] The nomenclature ''bonding'' and ''antibonding'' symmetry in the present context for diatomic or polyatomic molecules with symmetrically placed identical pairs of atoms refers to their MOs which could be expressed as a linear combination of sums or differences, respectively, of atomic orbitals on the symmetrically placed atomic pairs only.
[13] V.R. Bhardwaj, D.M. Rayner, D.M. Villeneuve, and P.B. Corkum, Phys. Rev. Lett. **87**, 253003 (2001).
[14] M. Lein, N. Hay, R. Velotta, J.P. Marangos, and P.L. Knight, Phys. Rev. Lett. **88**, 183903 (2002).
[15] M. Lein, N. Hay, R. Velotta, J.P. Marangos, and P.L. Knight, Phys. Rev. A **66**, 023805 (2002).
[16] B. Shan, X.M. Tong, Z. Zhao, Z. Chang, and C.D. Lin, Phys. Rev. A **66**, 061401(R) (2002).
[17] O.E. Alon, V. Averbukh, and N. Moiseyev, Phys. Rev. Lett. **80**, 3743 (1998).
[18] O.E. Alon, V. Averbukh, and N. Moiseyev, Phys. Rev. Lett. **85**, 5218 (2000).
[19] F. Ceccherini and D. Bauer, Phys. Rev. A **64**, 033423 (2001).
[20] M. Lein, P. Marangos, and P.L. Knight, Phys. Rev. A **66**, 051404(R) (2002).
[21] L.V. Keldysh, Zh. Éksp. Teor. Fiz. **47**, 1945 (1964) [Sov. Phys. JETP **20**, 1307 (1965)].
[22] F.H.M. Faisal, J. Phys. B **6**, L89 (1973).
[23] H.R. Reiss, Phys. Rev. A **22**, 1786 (1980).
[24] We may note here that intermediate resonances do not appear in the lowest order of the theory used here.
[25] A. Becker, L. Plaja, P. Moreno, M. Nurhuda, and F.H.M. Faisal, Phys. Rev. A **64**, 023408 (2001).
[26] F.H.M. Faisal, *Theory of Multiphoton Processes* (Plenum Press, New York, 1987).
[27] M.J. DeWitt, E. Wells, and R.R. Jones, Phys. Rev. Lett. **87**, 153001 (2001).
[28] E. Wells, M.J. DeWitt, and R.R. Jones, Phys. Rev. A **66**, 013409 (2002).
[29] K.P. Huber and G. Herzberg, *Constants of Diatomic Molecules*, in NIST Chemistry WebBook Vol. 69, edited by P.J. Lindstrom and W.G. Mallard (National Institute of Standards and Technology, Gaithersburg, MD, 2003) (webbook.nist.gov).
[30] A. van Orden and R.J. Saykally, Chem. Rev. (Washington, D.C.) **98**, 2313 (1998).
[31] Ch. Lifshitz, J. Mass Spectrom. **200**, 423 (2000).
[32] M.S. Deleuze, M.G. Giuffreda, J.-P. François, and L.S. Cederbaum, J. Chem. Phys. **111**, 5851 (1999).
[33] M.W. Schmidt *et al.*, J. Comput. Chem. **14**, 1347 (1993).
[34] K. Yabana and G.F. Bertsch, Z. Phys. D: At., Mol. Clusters **42**, 219 (1997).
[35] T. Berkus, P.-G. Reinhard, and E. Suraud, Int. J. Mol. Sci. **3**, 69 (2002).
[36] T. Seideman, Annu. Rev. Phys. Chem. **53**, 41 (2002).
[37] K.L. Reid, Annu. Rev. Phys. Chem. **54**, 397 (2003).
[38] A. Stolow, Annu. Rev. Phys. Chem. **54**, 89 (2003).
[39] I.V. Litvinyuk, K.F. Lee, P.W. Dooley, D.M. Rayner, D.M. Villeneuve, and P.B. Corkum, Phys. Rev. Lett. **90**, 233003 (2003).
[40] A. Talebpour, S. Larochelle, and S.L. Chin, J. Phys. B **31**, L49 (1998).
[41] A. Apalategui and A. Saenz, J. Phys. B **35**, 1909 (2002).
[42] The minimum number of photons N_0 required to ionize the molecule depends on the quiver energy $U_p = I/4\omega^2$. Thus, with increase of the intensity N_0 increases stepwise by one unit. This effect is called channel closing.